

**Topical Editor Decision: Publish subject to revisions (further review by editor and referees)** (29 Aug 2018) by Marc Salzmann

*Comments to the Author:*

*Thank you very much for including a revised manuscript in your response to the reviewers. It would have been enough to respond to the comments first and later submit a revised manuscript. But of course, a revised manuscript can help to make your points.*

**Dear Editor:** Thank you very much for your kindly comments and valuable suggestions, which help us to improve the quality of the paper. We have followed the editor's suggestions and the corresponding revision has been made (on the basis of the revised version according to reviewer #1 and reviewer #2). The changes we made are shown in red font. The revised manuscript with tracked changes is attached later.

*Based on your responses and the revised manuscript, my impression is that major comment #1 by reviewer number #1 and point #1 by reviewer #2 should be addressed by additional changes in the in the manuscript. The motivation for looking at ascents needs to be better explained in the manuscript. For example, you could include at least one or two sentences based on your response to reviewer #1 around line 104. If the motivation for your approach is made clear in the manuscript, personally I would not insist on changing the title, since it seems to express what you are intending to say. In general, however, it is often good to clarify things that are unclear in the manuscript, since not all readers may refer to the public discussion. Please note that there will be another opportunity to submit a revised manuscript and that this revised manuscript will be sent out for another round of reviews.*

**Response:** To make our points more clear, additional changes related to the choice of ascents are actually essential in the manuscript. According to your suggestions, changes have been made in the corresponding text. Please see lines 104-112, that is sentences “The research by Hocking et al., (2007) have achieved a development in this issue and reported that the rapid ascent in RT altitude ( $>0.2$  km/h) can be a valuable diagnostic for possible stratospheric intrusions. They observed the RT height started to ascent just when the stratospheric air intruded across the tropopause layer directly, although the ascent seems to be a recovery from the drop in tropopause height (many cases, not all, including this study). On the other hand, in fact, tropopause drops are more close related to various atmospheric processes such as cutoff low and low/high trough, rather than the corresponding intrusion process itself. Therefore, tropopause ascent is one of the key objects in this study.”

*I also noted that the first sentence of your acknowledgment seems to imply that your case study qualifies for the criterion in Raveh-Rubin (2017). If it is so, this should be explained (including a few details) in the main body of the manuscript and not in the acknowledgment section and there should definitely be a proper citation of Raveh-Rubin (2017).*

**Response:** Yes, Prof Raveh-Rubin helped us to check the case study using Lagrangian method, the case indeed qualifies for the criterion in Raveh-Rubin (2017). She found a large dry intrusion associated with the case of cut-off low. This has been mentioned in the revised manuscript, please see Lines 310-312, and a proper citation of Raveh-Rubin (2017) has been added. However, we must admit that we do not familiar with the Lagrangian method and criterion in Raveh-Rubin (2017).

*Non-public comments to the author:*

*I will be on vacation until 18 September, so please take your time and excuse me should it take me longer than usual to take a decision in case you submit the manuscript very soon.*

**Response:** Thank you very much again for your kindly and valuable comments. Also thank you very much for your quick decision. Personally, this paper is very important for me, because it relates to my doctor graduate directly.



23 stability of the radar tropopause seems to be weakened. Analysis results from global  
24 reanalysis and the satellite data, as well as the trajectory model have shown the clear  
25 evidence of the downward stratospheric intrusions (dry ozone-rich and depleted  
26 methane air) associated with the strong downdrafts. Twenty typical cases of such strong  
27 downdrafts, occurring during various synoptic processes in different seasons, have been  
28 presented and 15 of them are exactly associated with some form of stratospheric  
29 intrusions. Four years (2012-2015) of such downdrafts are further discussed. The  
30 observations reveal that the strong downdrafts preceding the rapid tropopause ascent  
31 can be a valuable diagnostic for monitoring intrusion events, which will gain a better  
32 understanding of stratospheric intrusions in VHF radar observations.

33

34 **Keywords:** Stratospheric intrusions; strong downdrafts; rapid tropopause ascent; MST  
35 radar; VHF radar; cut-off low

36

## 37 1. Introduction

38 The tropopause is a stable transition zone separating the vertically stable stratified  
39 stratosphere from the active free troposphere. The stratospheric and tropospheric air are  
40 remarkably different in their chemical and dynamical characteristics. The stratosphere  
41 is dominantly high in ozone and potential vorticity (PV) content and low in water vapor  
42 (WV) and methane (CH<sub>4</sub>) concentration, while the troposphere is just on the contrary  
43 (Holton et al., 1995). Consequently, the natural stable tropopause layer, characterized  
44 by strong gradients of trace constituents and wind speeds, plays an important role in  
45 stratosphere-troposphere exchange (STE) processes. In other words, the layer is a  
46 significant barrier for the atmospheric transport between stratosphere and troposphere  
47 (Mahlman, 1997). From a long-term point of view, the seasonal variation of the  
48 tropopause height determines the seasonal variation of the flux of stratospheric air into  
49 the free troposphere (Appenzeller et al., 1996). Under the global climate warming (e.g.  
50 the continuing rise in CO<sub>2</sub>), the tropopause variation is also a significant factor that  
51 must be considered with regards to the recovery of the stratospheric ozone (Butchart et  
52 al., 2010; Chipperfield et al., 2017). On the other hand, the short-term tropopause  
53 variability is sensitive to various meso- and small-scale atmospheric processes, during  
54 which the folding/intrusion events commonly occur. This characteristic of the  
55 tropopause change are sometimes directly used to detect the tropopause folds (e.g. Rao  
56 et al., 2008; Alexander et al., 2012, and references therein), but are less, if any, directly  
57 used to identify stratospheric intrusions. More detailed analysis of the variability of  
58 high-resolution tropopause height and of course some other parameters (e.g. 3-

59 dimensional wind), and how the stratospheric air is transported across the tropopause  
60 into the troposphere will help us to yield better understanding of the downward  
61 stratospheric intrusions (e.g. Sprenger et al., 2003; Leclair de Bellevue et al., 2007; Das  
62 et al., 2016).

63 Although photochemical production within the troposphere is the main source of  
64 tropospheric ozone, the influence of downward stratospheric intrusions on tropospheric  
65 ozone content cannot be ignored (Oltmans and Levy II, 1992; Stevenson et al., 2006).  
66 Stratospheric intrusions bring dry ozone-rich air down into the free troposphere (e.g.  
67 Stohl et al., 2000; Sørensen and Nielsen, 2001) and sometimes even deep to the surface  
68 (e.g. Gerasopoulos et al., 2006; Grant et al., 2008; Jiang et al., 2015; Das et al., 2016;).  
69 By now, it is well established that these intrusions of stratospheric origin will  
70 significantly influence other trace gases (such as hydroxyl (OH)) in the troposphere  
71 (Holton et al., 1995). These influences then will further contribute to the change of  
72 radiative balance (Ramaswamy et al., 1992) and play an important role in the radiative  
73 forcing of global climate change (Holton et al., 1995). It is true that stratospheric  
74 intrusion events occur all over the world and in any **seasons**. However, they are highly  
75 episodic in both vertical and isentropic (horizontal) directions (Chen, 1995). Various  
76 dynamical and physical processes have been proposed to be responsible for extra-  
77 tropical intrusion events. These mainly include tropopause folds, stratospheric  
78 streamers and break-up, cut-off lows (COLs), wave breaking, and mesoscale convective  
79 activities and thunderstorms (Stohl et al., 2003).

80 The certain dynamical and chemical characteristics of stratospheric air allow the

81 tracers, such as dry ozone-rich and high PV, to be proper indicators for the intrusions  
82 penetrating down into the troposphere. Based on these tracers, various **tools** are  
83 available to detect intrusion events. Balloon-borne ozonesonde sounding is an effective  
84 tool to make measurements of ozone with high vertical resolution, but is limited by  
85 coverage (He et al., 2011) and temporal resolution. In contrast, the satellite-borne  
86 remote sensing instruments, such as Atmospheric Infrared Sounder (AIRS), can provide  
87 nearly global coverage of various trace gases but have limitations in vertical and  
88 temporal resolution. Another method for studying transport processes is trajectory  
89 model, from which the backward trajectories can provide valuable information on the  
90 possible sources of the trace gases (e.g. Elbern et al., 1997).

91 By far, large-scale STE has been widely studied and is fairly well understood, but  
92 the details of small scale intrusions still need more researches (e.g. Holton et al., 1995).  
93 Kumar and Uma (2009) reported that the shortage of direct measurements of vertical  
94 winds near the tropopause may be responsible for the lack of fine-scale observations of  
95 smaller scale intrusions.

96 Very-High-Frequency (VHF) radars, compared to the tools mentioned above, are  
97 capable of continuously monitoring the atmosphere under any weather conditions and  
98 detecting tropopause height from backscattered signal with both high temporal and  
99 spatial resolution. During the past two decades, VHF radar measurements were  
100 commonly used to assist to study the stratospheric intrusions (e.g. Hocking et al., 2007;  
101 Das et al., 2016). However, it still remains uncertain in many aspects when using only  
102 the VHF radar to identify intrusion events, especially the criteria for the identification.

103 Complicated and changeable atmospheric processes make it difficult to identify the  
104 intrusion events by only radar data. The research by Hocking et al., (2007) have  
105 achieved a development in this issue and reported that the rapid ascent in RT altitude  
106 ( $>0.2$  km/h) can be a valuable diagnostic for possible stratospheric intrusions. They  
107 observed the RT height started to ascent just when the stratospheric air intruded across  
108 the tropopause layer directly, although the ascent seems to be a recovery from the drop  
109 in tropopause height (many cases, not all, including this study). On the other hand, in  
110 fact, tropopause drops are more close related to various atmospheric processes such as  
111 cutoff low and low/high trough, rather than the corresponding intrusion process itself.  
112 Therefore, tropopause ascent is one of the key objects in this study.

113 The central objective of the present study is to discuss the signature of downward  
114 cross-tropopause intrusions using both the measurements of tropopause height and  
115 vertical wind by the Beijing MST radar. This study is carried out mainly via a detailed  
116 case observation during the passage of a COL and other general cases associated with  
117 various atmospheric processes. Our discussion mainly focused on the potential of the  
118 MST radar data to identify possible intrusion events, which is the main point of this  
119 paper. In section 2 the datasets used in this paper are described, section 3 presents  
120 detailed results and discussion, and section 4 gives the conclusions.

121



## 122 2. Dataset

### 123 2.1. MST radar data and tropopause detection

124 The Beijing MST radar located at Xianghe, China (39.75° N, 116.96° E, 22 m  
125 above sea level) is a VHF radar operated at 50 MHz and installed in 2010 based on the  
126 first phase of Chinese Meridian Space Weather Monitoring Project (Chinese Meridian  
127 Project for short) (Wang, 2010). The radar antenna array consists of 24×24 three-  
128 element Yagi to produce an average power aperture product of  $3.2 \times 10^8 \text{ Wm}^2$  and  
129 maximum directive gain of 34.8 dB. It operates radiation pattern with 172 kW peak  
130 power and 3.2° half-power beam width. More detailed information of the radar system  
131 can be found in Chen et al. (2016). Routine low mode data were used for present study  
132 with 0.5 h time resolution and 1  $\mu\text{s}$  coded pulse, which provides 150 m vertical  
133 resolution. Details of the low mode setup used in this study are given in Table 1.

134 It has long been known that VHF radar reflectivity is proportional to the mean  
135 generalized refractive index gradient  $M$ , which is a function of humidity variation and  
136 static stability and given by (Ottersten, 1969) as follows

$$137 \quad M = -77.6 \times 10^{-6} (p/T) (d \ln \theta / dz) \\ 138 \quad \cdot \{ 1 + 15500 q / T [ 1 - (d \ln q / dz) / (2 d \ln \theta / dz) ] \} \quad (1)$$

139 where  $p$  is the atmospheric pressure (hPa)  $T$  is the temperature (K),  $\theta$  is the potential  
140 temperature (K) and  $q$  is the specific humidity ( $\text{gg}^{-1}$ ). According to the second and third  
141 terms of the equation (1): large humidity variation contributes to the echo from the  
142 lower and middle troposphere. From the first term: the radar backscatter power is  
143 proportional to the static stability, which in fact is directly proportional to the potential

144 temperature gradient. The tropopause, near which a strong potential temperature  
145 gradient exists, will lead to strong radar echoes in vertical incidence, as well as large  
146 radar aspect sensitivity (as shown in Figure 1). Radiosonde data used in this paper were  
147 received from the GTS1 type digital radiosonde launched from Beijing Meteorological  
148 Observatory (39.93 °N, 116.28 °E, station number 54511), which is less than 45 km  
149 away from the MST radar site. The black line in Fig. 1 denotes the lapse-rate tropopause  
150 (LRT) defined using the temperature lapse rate (World Meteorological Organization  
151 (WMO), 1986). Applying the characteristic (enhanced radar echoes due to partial  
152 specular reflection) mentioned above, the tropopause can be detected and its height  
153 determined by VHF radars (Gage and Green, 1979). It has received widespread  
154 application around the world, either in middle latitudes (e.g. Hocking et al., 2007), polar  
155 regions (e.g. Alexander et al., 2012), and tropical regions (e.g. Yamamoto et al., 2003;  
156 Das et al., 2008). Here, the radar-determined tropopause (RT) height is defined as the  
157 height (above 500 hPa) where the maximum vertical gradient of echo power located  
158 (shown as the orange circle in Figure 1a). This definition of RT is similar to that in the  
159 studies of Alexander et al., [2012] and Ravindrababu et al., [2014].

160 In the present study, the MST radar mainly provides continuous measurements of  
161 backscattered echo power, 3-D wind, and RT height with time resolution of 0.5 hour. In  
162 addition, the radar aspect sensitivity, expressed as the ratio between vertical ( $p_v$ ) and  
163 oblique ( $p_o$ , here used the 15-degree north) beam echo power, is mainly caused by the  
164 horizontally stratified anisotropic stable air and thus will be used as potential signature  
165 of stratospheric intrusions in the troposphere (e.g. Kim et al., 2001). The backscattered

166 echo power given here is expressed as relative power in decibels (dB). In order to reduce  
167 the random noise, the profile of  $p_v$  is smoothed by a 3-point running mean in altitude.  
168 Note that the data that are heavily contaminated will be eliminated from our datasets.  
169 The data of December 2015 and September 2015 are excluded.

## 170 2.2. AIRS satellite data

171 The AIRS instrument on NASA Aqua/EOS polar orbit satellite is a 2378 channel  
172 nadir cross-track scanning infrared spectrometer. It can provide profiles of a number of  
173 trace gases, including ozone and CH<sub>4</sub> (Susskind et al., 2003). The footprint of these  
174 retrieval data is of 45 km by 45 km and their most sensitive region is in an altitude range  
175 of 300-600 hPa. Many studies have shown that these AIRS retrieval constituents are  
176 useful indicators for detecting stratospheric intrusions. He et al. [2011] suggested that  
177 AIRS can observe the enhanced tropospheric ozone that is of stratospheric origin.  
178 Xiong et al. [2013] reported that AIRS is capable of observing abnormal depletion in  
179 CH<sub>4</sub> in the troposphere during intrusions. AIRS offers good latitude-longitude coverage.  
180 Here we use version 6 of the AIRS Level-3 ozone and methane retrieval products.

## 181 2.3. Meteorological reanalysis

182 European Centre for Medium-Range Weather Forecasts (ECMWF) reanalysis  
183 ERA-interim data are also used. After November 2000 the data are based on the  
184 T511L60 version available with a 6-h temporal resolution and  $3^\circ \times 3^\circ - 0.125^\circ \times$   
185  $0.125^\circ$  latitude-longitude grid (Dee et al., 2011). The dataset from 15 isentropic and  
186 37 pressure levels interpolated into  $0.5^\circ \times 0.5^\circ$  grid are applied for present study.

## 187 2.4. HYSPLIT model

188 Backward (forward) trajectories in given starting locations are capable to  
189 reproduce the sources (destinations) of the air parcel that will allow us to examine the  
190 intrusions of stratospheric origin in the troposphere (e.g. Elbern et al., 1997). The  
191 Hybrid Single Particle Lagrangian Integrated Trajectory model (HYSPLIT) developed  
192 by the National Oceanic and Atmospheric Administration (NOAA)'s Air Resource  
193 Laboratory (ARL) (Rolph, 2003; Stein et al., 2016) is applied to calculate the backward  
194 and forward trajectories. The calculation method of the model is a hybrid between the  
195 Lagrangian approach and the Eulerian methodology. In this paper, Global Data  
196 Assimilation System (GDAS) datasets are adopted for driving the HYSPLIT.  
197

198 **3. Results and discussion**

199 3.1. Meteorological synoptic situation

200 On the morning of 29 November 2014, a 500-hPa trough developed on the western  
201 side of Lake Baikal (Western Siberia). The trough moved southeastward and extended  
202 equatorward and its southern tip separated from the westerlies in the afternoon of 30  
203 November 2014 (Fig. 2b), forming a COL near the radar site as shown by the closed  
204 geopotential contour. The black stars in Figure 1 and other figures indicate the location  
205 of the radar site. On the following days, the COL system moved northeastward  
206 gradually (Fig. 2b) and finally stayed over eastern Russia near Sakhalin Island until it  
207 reconnected and merged to the westerly flow. 315 K isentropic PV patterns have shown  
208 the coarse resolution features of intrusions from the polar reservoir across the  
209 tropopause into the midlatitude troposphere. The PV streamer curved and rolled up  
210 cyclonically along the western flank of the COL (Fig. 2b).

211 Fig. 3 shows the time series of hourly surface meteorological parameters over the  
212 Beijing station. The data are obtained from the Chinese National Meteorology  
213 Information Center and is less than 50 km from the MST radar site. As the dry-cold air  
214 invasion accompanied with the COL travelled deeply into the planetary boundary layer,  
215 it brought severe weather to the surface, including a rapid decrease in temperature and  
216 humidity, and rapid increase in surface wind and sea level pressure. The humidity  
217 decreased from ~85 to 12 percent within less than 8 hours. It is well established that the  
218 polar-type COLs have strong potential to trigger deep convection (Price and Vaughan,  
219 1993). To examine the potential convection, maps of high quality Climate Data Record

220 (CDR) of daily Outgoing Longwave Radiation (OLR) are displayed in Fig. 4. During  
221 the development of the COL, a local region with abnormal low OLR value was clearly  
222 observed near the radar site on 29 November (Fig. 4b). The Satellite-observed cloud  
223 top temperature also showed the low values corresponding to the low OLR (figure not  
224 shown), indicating that convection may be generated near radar side on 29 November.  
225 Please note that we did not observe such low value either in OLR (Fig.4c, d) or in cloud  
226 top temperature near the radar side on 30 November and 1 December. The time for all  
227 the observations in this paper is shown in Universal Time (UTC) which is eight hours  
228 behind Beijing standard time (LT=UTC+8).

### 229 **3.2. MST radar observations**

230 Radar echo power, horizontal wind vector, vertical wind, and radar aspect  
231 sensitivity are plotted in Figure 5 as function of height and time during the passage of  
232 the COL. Time variation of RT (black line) and LRT (black crosses) heights are also  
233 displayed. The RT height first experienced a rapid descent, and then increased rapidly,  
234 forming a deep V-shaped structure of ~4 km depth. The vertical velocity of the RT  
235 height variation (both the rapid descent and ascent branches) reaches up to 0.28 km/h.  
236 The rapid RT variation in altitude is in fact the response of the tropopause fold below  
237 the jet stream, which will be well represented in Fig. 8a. Rapid variation in RT height  
238 remained a region with low echo power (marked by R on Fig. 5a) and low aspect  
239 sensitivity (marked by R' on Fig. 5d) where they should be normally high value within  
240 the 'normal' tropopause layer. Unlike the RT height, the radiosonde LRT altitudes are  
241 nearly constant during the COL passage. In normal conditions, RT agrees well with the

242 LRT altitude, such as indicated by Fig. 6a. However, large differences, of order of 2.5  
243 km (as shown in Fig. 6b at 12 UTC 30 November), are observed between LRT and RT  
244 in altitude during the passage of the COL as expected. It is the difference in definition  
245 that contribute most to the large differences, especially under the tropopause fold  
246 conditions (e.g. Yamamoto et al., 2003 and Fukao et al., 2003). It is worth noting that,  
247 in Fig.6b, although there is no clear reversion in the radiosonde temperature profile  
248 within the height of RT, the RT height exactly corresponds well to the reversion of  
249 zonal and meridional wind and potential temperature gradient. Such differences  
250 between RT and LRT heights can commonly be observed, especially during extreme  
251 synoptic situations such as cyclone (e.g. Alexander et al., 2012).

252 The most important observation in this detailed case experiment is the strong  
253 downdrafts (hereinafter inferred to as main downdrafts) observed immediately  
254 preceding the rapid RT ascent (Fig.5c). The radar echo power sharply weakened (dotted  
255 rectangle in Fig.5a) and the wind direction changed rapidly (Fig.5b, change from  
256 dominant southerly wind to dominant northerly jet) within the height region of the main  
257 downdrafts. As mentioned previously, abnormal low value in OLR and cloud top  
258 temperature indicates the possible occurrence of convective activity on 29 November,  
259 but nothing special appeared on 30 November near radar site. Consequently, we  
260 preliminarily consider that the main downdrafts occurred near 07 UT 30 November  
261 might not be produced directly by convective activity. Here, the accurate origin of the  
262 main downdrafts will not be discussed in detail, and it is also beyond the scope of  
263 present study.

264 The research by Hocking et al. (2007) has suggested that the rapid ascent in RT  
265 height ( $>0.2 \text{ km h}^{-1}$ ) can be a valuable predictor for the occurrence of stratospheric  
266 intrusions. Here in this paper, the main downdrafts preceding the rapid RT ascent  
267 observed by the Beijing MST radar are thus suspected to be an important feature or  
268 response of some form of vertical stratospheric intrusions. Firstly, as the tropopause  
269 descends (folded downward), it will displace stratospheric air into the troposphere (e.g.  
270 Hoskins et al., 1985). Secondly, the main downdrafts will act as an effective way to  
271 weaken the tropopause by means of continuously impinging on the tropopause, through  
272 which the stratospheric air is permitted to penetrate down into the free troposphere (e.g.  
273 Hirschberg and Fritsch, 1993; Kumar, 2006). In addition, after the main downdrafts,  
274 the observed region near the upper troposphere with strong backscatter echoes (marked  
275 by Q) and especially with abnormal high aspect sensitivity (marked by Q') may also be  
276 a weak signature of the possible intrusions. In normal conditions, they are usually low  
277 in value in the upper-troposphere (such as the region marked by P and P'). As we  
278 mentioned before, the large value in radar aspect sensitivity is mainly caused by  
279 reflection from stable atmospheric layer, such as the tropopause or lower-stratosphere.  
280 When stable stratospheric air intrudes into the troposphere and without mixing with the  
281 surrounding air mass, the intrusions in the free troposphere will be reflected as abnormal  
282 large aspect sensitivity. Further direct evidence of the relevant intrusions in dynamical  
283 and chemical aspects will be demonstrated in next section, using satellite AIRS and  
284 global reanalysis data.

### 285 3.3. Associated stratospheric intrusions



286 Due to the sensitivity of the AIRS retrieved ozone and CH<sub>4</sub> is between 300-600  
287 hPa. Fig. 7 shows the 500 hPa distribution of AIRS observed ozone and CH<sub>4</sub>, along  
288 with the AIRS tropopause contour (defined based on the temperature lapse-rate). The  
289 ozone distribution maps (left panels of Fig. 7) clearly show a large area with enhanced  
290 tropospheric ozone (>80 ppbv) near the radar site during the passage of the COL.  
291 Moreover, severe CH<sub>4</sub> depletion (<1840 ppbv) was also observed (right panels in Fig.  
292 7). These features of the ozone enhancement, CH<sub>4</sub> depletion, and the corresponding low  
293 tropopause altitude clearly support the evidence of vertical downward cross-tropopause  
294 stratospheric intrusions on 30 November.

295 The vertical cross-section of ECMWF PV and specific humidity at 1800 UT 30  
296 November 2014 and the daily AIRS ozone on 30 November 2014, along a constant  
297 latitude 40° N, is shown in Fig. 8. The corresponding vertical structure of the  
298 stratospheric intrusions (dry ozone-rich and high PV along with low tropopause) over  
299 regions near radar side is clearly seen. The specific humidity tracer displays less distinct  
300 structure as compared with the other two tracers (similar as that shown by Vérémes et  
301 al., 2016). The cross-section of PV in Fig. 8a have demonstrated relatively finer-scale  
302 structure of the stratospheric PV intrusions (below the jet stream), which penetrated  
303 down deeply into ~650 hPa (~3.6 km).

304

#### 305 3.4. Trajectory model analysis

306 Figure 9 shows 30h backward trajectories ending at the radar site at 18 UT 29  
307 November (left panel) and at 18 UT 30 November (right panel). As expected, the air

308 masses parcel transported eastward horizontally before the occurrence of main  
309 downdrafts (Fig. 9a). Whereas after the downdrafts, the trajectories clearly show  
310 downward intrusions originated from the western side of Lake Baikal. Furthermore, a  
311 huge dry intrusion is tracked according to the criterion (based on Lagrangian method)  
312 in Raveh-Rubin (2017). Trajectory results further support the evidence of possible  
313 stratospheric intrusions that closely related with the main downdrafts.

314 On the other hand, 30-h forward trajectories starting at 00 UT 30 November (left  
315 panel) and 00 UT 1 December (right panel) are shown in Fig. 10. It is interesting to note  
316 that, from Fig. 10a before the passage of COL, the air parcels at 4 km transport rapidly  
317 upward (by more than 4 km within ~23 h) and northeastward to the upper-troposphere  
318 of East Siberian. This upward and poleward transportation is associated with a warm  
319 conveyor belt (southerly flows dominate) that is located ahead of the COL. It  
320 contributes to transporting the tropospheric moist and polluted air (such as aerosol) into  
321 the upper-troposphere and even the lower stratosphere (e.g. Stohl et al., 2003; Sandhya  
322 et al., 2015). After the downdrafts, forward trajectories in Fig. 10b demonstrate that the  
323 dry intrusion air parcels continue to be transported downward and southeastward to the  
324 boundary layer or even the surface.

### 325 3.5. Strong downdrafts preceding rapid tropopause ascent and discussion

326 Figure 11a shows another 20 typical cases of strong downdrafts preceding rapid  
327 RT ascent for the period March 2012 and Jan. 2015 (shown placed end-to-end), the  
328 LRT height (plotted in crosses) and the vertical velocity of the RT (plotted in orange  
329 line) is also plotted. These cases (marked by black rectangular boxes and labeled as S1,

330 S2, S3..., and S20) are identified based on the following criteria: 1) the amplitude of  
331 the RT ascent should exceed 0.6 km (four range gates), 2) vertical velocities of the RT  
332 ascent excess 0.1 km/h, 3) the downdrafts occurred preceding the RT ascent should >0.5  
333 m/s, and the height region of the downdrafts should pass through the RT layer. The  
334 criteria are put forward mainly to avoid the influence of the RT spikes. Figure 11b  
335 shows the backward trajectories for the selected 9 cases. Results show clear evidence  
336 of downward intrusions corresponding to the associated strong downdrafts. Their  
337 sources are mainly from West Siberia (western side of Lake Baikal), except for the case  
338 Tr5. Moreover, according to AIRS daily 500 hPa ozone distribution, most of the cases  
339 in Figure 11a (except for the cases S14, S15, S16, S17, S20) were associated with  
340 significant ozone enhancement, indicating intrusions of stratospheric origin (as shown  
341 in Supplementary figure S1). It is important to note that the RT excursion velocity of  
342 all the cases is not all above 0.2 km/h and some are lower than this value (e.g. cases  
343 S16 and S18). However, some form of stratospheric intrusions was exactly observed in  
344 such cases from both the trajectory and satellite results. Therefore, the threshold of  
345 vertical velocity of the RT ascent is set at 0.1 km/h, rather than 0.2 km/h (Hocking et  
346 al., 2007). Large differences between RT and LRT are also interesting to be noted on  
347 some occasions when the RT changes rapidly (such as the occasion near 14 March  
348 2012).

349 According to the meteorological chart, the synoptic situation of those cases  
350 identified in Fig. 11a are introduced. The cases S1, S2, S8, S9, S10, and S11 seem to  
351 have a close relationship with COL development; cases S3, S4, S5, S6, S7, S17, S18,

352 and S19 seem associated with low or high trough systems (at 500 hPa). The remaining  
353 cases seem not associated with any significant synoptic development. However, in  
354 terms of the distribution of isentropic PV (generally at 315K in winter and 330K in  
355 summer), we found that the remaining cases S12, S13, S14, S15, S16, and S20 appear  
356 to be associated with some form of stratospheric streamers and their break-up within  
357 the previous 48h (not shown). Some cases (e.g. S1 and S2) that appear close on the  
358 same day were probably caused by the same system. The characteristics of the 20 cases,  
359 including background synoptic condition, vertical velocity of the RT ascent, and 500  
360 hPa ozone enhancement, have been summarized in Table 2.

361 In the light of present understanding, the strong downdrafts preceding the rapid  
362 RT ascent can serve as an important diagnostic for intrusion events, during various  
363 synoptic processes in any season. This characteristic will be of great use and play an  
364 important role in routine identification of stratospheric intrusions. Considering the  
365 duration of such downdrafts, a higher time resolution of radar observations will be more  
366 helpful. Present study has shown the duration of the majority downdrafts is generally  
367 within 1.5-3 hours. We consider, therefore, that the radar resolution should be best  
368 within 1h.

369 Although Hocking et al. (2007) have reported that the rapid tropopause ascent  
370 ( $>0.2$  km/h) alone can be a useful diagnostic for potential intrusion events. However,  
371 using only the information of RT heights might lead to non-negligible errors, as  
372 mentioned above in introduction and according to the observations in Fig. 11.  
373 Especially on occasions when the RT ascent is between 0.1-0.2 km/h but the

374 corresponding true intrusions were observed, all such intrusion events will be neglected  
375 (maybe ~2 per month, refer to Fig. 12a). Whereas on some occasions when the RT  
376 ascent exceeds 0.2 km/h, but without observing true intrusion events (e.g. He et al.,  
377 2011), these events will be misdiagnosed (maybe ~13 per month, refer to Fig. 12b). In  
378 this sense, using the unique MST radar observations of both the RT height variability  
379 and the vertical wind as complementary signature for identifying possible intrusion  
380 events is very meaningful.

381 Figure 12 shows four years (2012-2015) of the events with rapid RT ascent (gray  
382 bands), and the events with strong downdrafts just preceding the rapid RT ascent (black  
383 bands). The identification criteria of such strong downdrafts are similar to that  
384 mentioned above and the events are classified according to different value of vertical  
385 velocity of the ascent. Among all the events with ascent velocity between 0.1-0.2 km/  
386 h, about one-quarter (approximate 2 per month, Fig. 12a) were observed with strong  
387 downdrafts preceding them. Whereas, as for the events with the ascent velocity >0.2  
388 km/h, the proportion is about a half (approximate 10 per month, Fig. 12b). Here,  
389 according to the results above, the occurrence of the strong downdrafts just preceding  
390 the rapid RT ascent (black bands in Fig. 12) to a large degree represents the occurrence  
391 of possible intrusions. In this way, Fig. 12 indicates that the occurrence of possible  
392 intrusions exhibit distinct seasonal variations, with a maximum in winter and spring  
393 minimum in summer. This is because the meso- and small-scale atmospheric processes,  
394 such as cold air outbreaks, thunderstorms, and convective activities, are more active in  
395 winter and spring. They are important sources for downward stratospheric intrusions.



397 **4. Conclusions**

398 Detailed case analysis of the cross-tropopause stratospheric intrusions was carried  
399 out during a COL. Global reanalysis, satellite data, and HYSPLIT trajectories all  
400 showed consistent evidences of dry ozone-rich, high PV, and depleted CH<sub>4</sub> air that have  
401 penetrated downward into the free troposphere. The key signature of the stratospheric  
402 intrusions in the Beijing MST radar observations is the strong downdrafts just preceding  
403 rapid RT ascent. The radar echo power decreased rapidly within the region of strong  
404 downdrafts, after which abnormal high aspect sensitivity was recorded in troposphere.  
405 Such high aspect sensitivity is served as another potential clue for the intrusions of  
406 stratospheric origin.

407 Based on the criteria mentioned in section 3.5, other 20 typical cases of strong  
408 downdrafts preceding the rapid RT ascent between March 2012 and January 2015 were  
409 presented. These events occurred during different synoptic processes in different  
410 seasons. Yet, most of the cases (15 of them) are associated with some form of intrusions  
411 observed by combination of AIRS-retrieved ozone and the HYSPLIT trajectory model.  
412 Our results show that the radar-derived tropopause height and vertical winds are strong  
413 complementary indicators to be used to infer the occurrence of the intrusions of  
414 stratospheric origin. This will be of great use and play an important role for the routine  
415 identification or prediction of intrusion events. However, the actual origin of the  
416 observed downdrafts preceding the rapid RT ascent is not addressed in this paper.  
417 Further combination observational experiments need to be conducted, especially  
418 combined using ozonesonde soundings, to quantitative analyze the effectiveness of

419 present identification criteria for possible intrusions.

420

421



422 **Acknowledgment**

423 The authors really appreciate Prof Shira Raveh-Rubin for reading and checking the  
424 manuscript. This work is funded by National Natural Science Foundation of China  
425 (NSFC grants No. 41722404 and 41474132). The authors would like to thanks the  
426 technical and scientific staff of Chinese Meridian Space Weather Monitoring Project  
427 (CMSWMP) for their support in conducting the experiment. The authors sincerely  
428 acknowledge the ECMWF, NASA, and NOAA Air Resources Laboratory (ARL) for  
429 providing global reanalysis, satellite trace gases, and HYSPLIT transport model,  
430 respectively. The MST radar data for this paper are available at Data Centre for  
431 Meridian Space Weather Monitoring Project (<http://159.226.22.74/>). The radiosonde  
432 data is available from <http://weather.uwyo.edu/upperair/sounding.html>.

433

434 **References**

435 Appenzeller, C., Holton, J. R., & Rosenlof, K. H.: Seasonal variation of mass transport  
436 across the tropopause. *Journal of Geophysical Research Atmospheres*, 101(D10),  
437 15071–15078, 1996.

438 Appenzeller, C., Davies, H. C., & Norton, W. A.: Fragmentation of stratospheric  
439 intrusions. *Journal of Geophysical Research Atmospheres*. 101(D1), 1435-1456,  
440 1996.

441 Alexander, S. P., Murphy, D. J., and Klekociuk, A. R.: High resolution VHF radar  
442 measurements of tropopause structure and variability at Davis, Antarctica (69° S,  
443 78° E). *Atmospheric Chemistry and Physics*, 13(12), 26173-26205, 2012.

444 Bonasoni, P., Evangelisti, F., Bonafe, U., Ravegnani, F., Calzolari, F., Stohl, A., Tositti  
445 L., Tubertini O., & Colombo, T.: Stratospheric ozone intrusion episodes recorded  
446 at Mt. Cimone during the VOTALP project: case studies. *Atmospheric*  
447 *Environment*, 34(9), 1355-1365, 2000.

448 Butchart, N., Cionni, I., Eyring, V., Shepherd, T. G., Waugh, D. W., & Akiyoshi, H., et  
449 al.: Chemistry-climate model simulations of twenty-first century stratospheric  
450 climate and circulation changes. *Journal of Climate*, 23(20), 5349-5374, 2010.

451 Chipperfield, M. P., Bekki, S., Dhomse, S., Harris, N., Hassler, B., & Hossaini, R., et  
452 al.: Detecting recovery of the stratospheric ozone layer. *Nature*, 549(7671), 211-  
453 218, 2017.

454 Chen, P.: Isentropic cross-tropopause mass exchange in the extratropics. *Journal of*  
455 *Geophysical Research*, 16661-16673, 1995.

456 Chen, G., Cui, X., Chen, F., Zhao, Z., Wang, Y., Yao, Q., ... & Gong, W.: MST Radars  
457 of Chinese Meridian Project: System Description and Atmospheric Wind  
458 Measurement. *IEEE Transactions on Geoscience and Remote Sensing*, 54(8),  
459 4513-4523, 2016.

460 Das, S. S., A. R. Jain, K. K. Kumar, and D. Narayana Rao: Diurnal variability of the  
461 tropical tropopause: Significance of VHF radar measurements, *Radio Sci.*, 43,  
462 RS6003, doi:10.1029/2008RS003824, 2008.

463 Das, S. S., Ratnam, M. V., Uma, K. N., Patra, A. K., Subrahmanyam, K. V., Girach, I.  
464 A., Suneeth K. V. , Kumar K. K., & Ramkumar, G.: Stratospheric intrusion into  
465 the troposphere during the tropical cyclone Nilam (2012). *Quarterly Journal of the*  
466 *Royal Meteorological Society*, 142(698), 2168-2179, 2012.

467 Das, S.S., M. V. Ratnam, K. N. Uma, K. V. Subrahmanyam, I.A.Girach, A. K. Patra,S.  
468 Aneesh, K.V. Suneeth, K. K. Kumar, A.P.Kesarkar, S. Sijikumar and G.  
469 RamkuMarch.: Influence of Tropical Cyclones on Tropospheric Ozone: Possible  
470 Implications (2016), *Atmospheric Chemistry and Physics*, 16, 4837-4847, 2016.

471 Dee, D. P., Uppala, S. M., Simmons, A. J., Berrisford, P., Poli, P., & Kobayashi, S., et  
472 al.: The era-interim reanalysis: configuration and performance of the data  
473 assimilation system. *Quarterly Journal of the Royal Meteorological Society*,  
474 137(656), 553-597, 2011.

475 Elbern, H., Kowol, J., Sládkovic, R., & Ebel, A.: Deep stratospheric intrusions: a  
476 statistical assessment with model guided analyses. *Atmospheric Environment*,  
477 31(19), 3207-3226, 2006.

478 Fukao, S., H. Hashiguchi, M. Yamamoto, T. Tsuda, T. Nakamura, M. K. Yamamoto,  
479 T. Sato, M. Hagio, and Y. Yabugaki.: Equatorial Atmosphere Radar (EAR).:  
480 System description and first results, *Radio Sci.*, 38(3), 1053,  
481 doi:10.1029/2002RS002767, 2003.

482 Gage, K. S., & Green, J. L.: Tropopause detection by partial specular reflection with  
483 Very-High-Frequency radar. *Science*, 203(4386), 1238-40, 1979.

484 Gerasopoulos, E., Zanis, P., Papastefanou, C., Zerefos, C.S., Ioannidou, A., Wernli, H.:  
485 A complex case study of down to the surface intrusions of persistent stratospheric  
486 air over the Eastern Mediterranean. *Atmospheric Environment*, 40(22), 4113-4125,  
487 2006.

488 Grant, Deanne, Jose D. Fuentes, Marcia S. DeLonge, Stephen Chan, Everette Joseph,  
489 Paul Kucera, Seydi A. Ndiaye, Amadou T. Gaye (2008), Ozone transport by  
490 mesoscale convective storms in western Senegal, *Atmos. Envir.*, 42, 7104–7114,  
491 doi:10.1016/j.atmosenv.2008.05.044

492 He, H., Tarasick, D. W., Hocking, W. K., Careysmith, T. K., Rochon, Y. J., Zhang, J., ...  
493 & Bourqui, M. S.: Transport analysis of ozone enhancement in Southern Ontario  
494 during BAQS-Met. *Atmospheric Chemistry and Physics*, 11(6), 2569-2583, 2011.

495 Hocking, W. K., Careysmith, T., Tarasick, D. W., Argall, P. S., Strong, K., Rochon, Y.  
496 J., Zawadzki Irek & Taylor, P. A.: Detection of stratospheric ozone intrusions by  
497 windprofiler radars. *Nature*, 450(7167), 281-284, 2007.

498 Holton, J. R., P. H. Haynes, M. E. McIntyre, A. R. Douglass, R. B. Rood, and L. Pfister:  
499 Stratosphere-troposphere exchange, *Reviews of Geophysics*, 33(4), 403–439,

500       doi:10.1029/95RG02097, 1995.

501   Hoskins B.J., McIntyre M.E., Robertson A.W.: On the use and significance of  
502       isentropic potential vorticity maps. *Q. J. R. Meteorol. Soc.* 111: 877–946. 1985.

503   Hirschberg, P. A., and J. M. Fritsch: A study of the development of extratropical  
504       cyclones with an analytic model. Part I: The effects of stratospheric structure,  
505       *Journal of the Atmospheric Sciences*, 50, 311 –327, doi:10.1175/1520-  
506       0469(1993)050<0311:ASOTDO>2.0.CO;2, 1993.

507   Jiang, Y. C., T. L. Zhao, J. Liu, X. D. Xu, C. H. Tan, X. H. Cheng, X. Y. Bi<sup>6</sup>, J. B. Gan,  
508       J. F. You, and S. Z. Zhao (2015), Why does surface ozone peak before a typhoon  
509       landing in southeast China? *Atmos. Chem. Phys.*, 15, 13331–13338,  
510       doi:10.5194/acp-15- 13331-2015

511   Kim, K. E., Jung, E. S., Campistron, B., & Heo, B. H.: A physical examination of  
512       tropopause height and stratospheric air intrusion: a case study. *Journal of the*  
513       *Meteorological Society of Japan*, 79(5), 1093-1103, 2001.

514   Kumar, K. K., & Uma, K. N.: High temporal resolution VHF radar observations of  
515       stratospheric air intrusions in to the upper troposphere during the passage of a  
516       mesoscale convective system over gadanki (13.5° n, 79.2° e). *Atmospheric*  
517       *Chemistry & Physics*, 24(8), 14-17, 2009.

518   Kumar, K. K.: VHF radar observations of convectively generated gravity waves: Some  
519       new insights. *Geophysical Research Letters*, 33(1), doi:10.1029/2005GL024109,  
520       2006.

521   Leclair de Bellevue J, Baray JL, Baldy S, Ancellet G, Diab R, Ravetta F.: Simulations

522 of stratospheric to tropospheric transport during the tropical cyclone Marlene  
523 event. *Atmospheric Environment*. **41**: 6510–6526, 2007.

524 Mahlman, J. D.: Dynamics of transport processes in the upper troposphere. *Science*,  
525 276(5315), 1079-1083, 1997.

526 Mihalikova, M., Kirkwood, S., Arnault, J., & Mikhaylova, D.: Observation of a  
527 tropopause fold by MARA VHF wind-profiler radar and ozonesonde at Wasa,  
528 Antarctica: comparison with ECMWF analysis and a WRF model simulation.  
529 *Annales Geophysicae*, 30(9), 1411-1421, 2012.

530 Nastrom, G. D., Green, J. L., Gage, K. S., & Peterson, M. R.: Tropopause folding and  
531 the variability of the tropopause height as seen by the flatland VHF radar. *Journal*  
532 *of Applied Meteorology*, 28(12), 1271-1281, 1989.

533 Oltmans, S. J., and H. Levy II.: Seasonal cycle of surface ozone over the western North  
534 Atlantic, *Nature*, 358, 392–394, 1992.

535 Ottersten, H.: Mean vertical gradient of potential refractive index in turbulent mixing  
536 and radar detection of CAT, *Radio Science*, 4, 1247–1249,  
537 doi:10.1029/RS004i012p01247, 1969.

538 Price, J. D., & Vaughan, G.: The potential for stratosphere-troposphere exchange in cut-  
539 off-low systems. *Quarterly Journal of the Royal Meteorological Society*, 119(510),  
540 343-365, 1993.

541 Rao, T. N., and S. Kirkwood: Characteristics of tropopause folds over Arctic latitudes,  
542 *Journal of Geophysical Research*, 110, D18102, doi:10.1029/2004JD005374,  
543 2005.

544 Rao, T. N., Arvelius, J., & Kirkwood, S.: Climatology of tropopause folds over a  
545 European arctic station (esrange). *Journal of Geophysical Research Atmospheres*,  
546 113(D7), 762-770, 2008.

547 Ravindrababu, S., Venkat Ratnam, M., Sunilkumar, S. V., Parameswaran, K., and  
548 Krishna Murthy, B. V.: Detection of tropopause altitude using Indian MST radar  
549 data and comparison with simultaneous radiosonde observations. *Journal of*  
550 *Atmospheric and Solar-Terrestrial Physics*, 121(6), 679-687, 2014.

551 Ramaswamy V, Schwarzkopf MD, Shine KP.: Radiative forcing of climate from  
552 halocarbon-induced global stratospheric ozone loss. *Nature* **355**: 810–812, doi:  
553 10.1038/355810a0, 1992.

554 Rolph, G.D.: Real-time Environmental Applications and Display sYstem (READY)  
555 Website. NOAA Air Resources Laboratory, Silver Spring, MD. [http://](http://www.arl.noaa.gov/ready/hysplit4.html)  
556 [www.arl.noaa.gov/ready/hysplit4.html](http://www.arl.noaa.gov/ready/hysplit4.html), 2003.

557 **Raveh-Rubin, S.: Dry Intrusions: Lagrangian Climatology and Dynamical Impact on**  
558 **the Planetary Boundary Layer. *J. Climate*, 30, 6661–6682, 2017.**

559 Sandhya, M., Sridharan, S., & Indira Devi, M.: Tropical upper tropospheric humidity  
560 variations due to potential vorticity intrusions. *Annales Geophysicae*, 33(9), 1081-  
561 1089, 2015.

562 Skerlak, B., Sprenger, M., Pfahl, S., Tyrlis, E., & Wernli, H.: Tropopause folds in ERA-  
563 Interim: Global climatology and relation to extreme weather events. *Journal of*  
564 *Geophysical Research*, 120(10), 4860-4877, 2015.

565 Stohl, A., Bonasoni, P., Cristofanelli, P., Collins, W., Feichter, J., & Frank, A., et al.:

566 Stratosphere-troposphere exchange: a review, and what we have learned from  
567 staccato. *Journal of Geophysical Research Atmospheres*, 108(D12), 469-474, 2003.

568 Stohl, A., et al.: The influence of stratospheric intrusions on alpine ozone concentrations,  
569 *Atmospheric Environment*, 34, 1323– 1354, 2000.

570 Stohl, A., Wernli, H., James, P., Bourqui, M., Forster, C., & Liniger, M. A., et al.: A new  
571 perspective of stratosphere troposphere exchange. *Bulletin of the American*  
572 *Meteorological Society*, 84(11), 2003.

573 Stein, A. F., Draxler, R. R., Rolph, G. D., Stunder, B. J. B., Cohen, M. D., & Ngan, F.:  
574 NOAA's HYSPLIT atmospheric transport and dispersion modeling system. *Bulletin*  
575 *of the American Meteorological Society*, 96(12), 150504130527006, 2016.

576 Stevenson, D. S., Dentener, F. J., Schultz, M. G., Ellingsen, K., Noije, T. P. C. V., &  
577 Wild, O., et al.: Multimodel ensemble simulations of present-day and near-future  
578 tropospheric ozone. *Journal of Geophysical Research Atmospheres*, 111(D8), 263-  
579 269, 2006.

580 Sørensen, J. H., and Nielsen, N. W.: Intrusion of stratospheric ozone to the free  
581 troposphere through tropopause folds -a case study. *Physics and Chemistry of the*  
582 *Earth Part B Hydrology Oceans and Atmosphere*, 26(10), 801-806, 2001.

583 Su, L., Yuan, Z., Fung, J. C., & Lau, A. K.: A comparison of HYSPLIT backward  
584 trajectories generated from two GDAS datasets. *Science of The Total Environment*,  
585 527-537, 2015.

586 Susskind, J., C. D. Barnett, and J. M. Blaisdell.: Retrieval of atmospheric and surface  
587 parameters from AIRS/AMSU/HSB data in the presence of clouds, *IEEE*



588 Transactions on Geoscience and Remote Sensing, 41(2), 390–409,  
589 doi:10.1109/tgrs.2002.808236, 2003.

590 Vaughan, G., Gouget, H., O’Connor, F. M., & Wier, D.: Fine-scale layering on the edge  
591 of a stratospheric intrusion. *Atmospheric Environment*, 35(12), 2215–2221, 2001.

592 Vèrèmes, H., J.-P. Cammas, J.-L. Baray, P. Keckhut, C. Barthe, F. Posny, P. Tulet, D.  
593 Dionisi, and S. Bielli: Multiple subtropical stratospheric intrusions over Reunion  
594 Island: Observational, Lagrangian, and Eulerian numerical modeling approaches,  
595 *Journal of Geophysical Research Atmospheres*, 121, 14,414–14,432, doi:10.1002/  
596 2016JD025330, 2016.

597 Wang, C.: New Chains of Space Weather Monitoring Stations in China. *Space Weather-*  
598 *the International Journal of Research and Applications*, 8(8), 2010.

599 World Meteorological Organization (WMO): Atmospheric ozone 1985, WMO Global  
600 Ozone Res. and Monit. Proj. Rep. 20, Geneva, Switzerland, 1986.

601 Xiong, X., C. Barnet, E. Maddy, S. C. Wofsy, L. Chen, A. Karion, and C. Sweeney.:  
602 Detection of methane depletion associated with stratospheric intrusion by  
603 atmospheric infrared sounder (AIRS), *Geophysical Research Letters*, 40, 2455–  
604 2459, doi:10.1002/grl.50476, 2013.

605 Yamamoto, M., Oyamatsu, M., Horinouchi, T., Hashiguchi, H., & Fukao, S.: High time  
606 resolution determination of the tropical tropopause by the Equatorial Atmosphere  
607 Radar. *Geophysical Research Letters*, 30(21), 2003.

608

**Table**

Radar parameter	Value
Transmitted frequency	50 MHz
Antenna array	24×24 3-element Yagi
Antenna gain	33 dB
Transmitter peak power	172.8 kW
Code	16-bit complementary
No. coherent integrations	128
No. FFT points	256
No. spectral average	10
Pulse repetition period	160 $\mu$ s
Half power beam width	3.2°
Pulse length	1 $\mu$ s
Range resolution	150 m
Temporal resolution	30 min
Off-zenith angle	15°

610 **Table 1.** Operating parameters in low-mode of the Beijing MST radar.

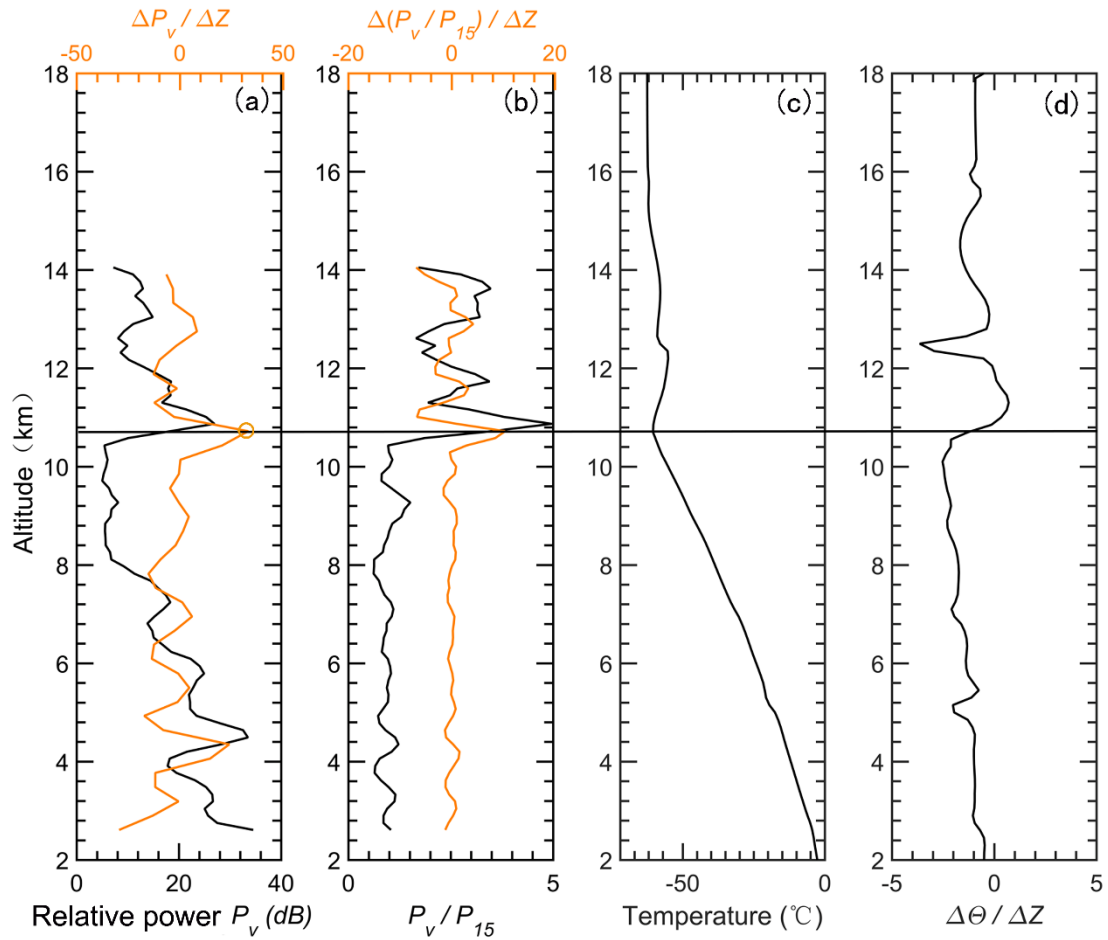
611

Cases	Time (year/month/day)	Background condition	Vertical velocity of RT ascent	500 hPa ozone enhancement
S1	2012/03/06	Cut-off low	>0.2 km/h	Enhanced
S2	2012/03/06	Cut-off low	>0.2 km/h	Enhanced
S3	2012/03/12	Low/high trough	>0.2 km/h	Enhanced
S4	2012/03/13	Low/high trough	>0.2 km/h	Enhanced
S5	2012/04/05	Low/high trough	>0.2 km/h	Enhanced
S6	2012/04/05	Low/high trough	>0.2 km/h	Enhanced
S7	2012/04/06	Low/high trough	>0.2 km/h	Enhanced
S8	2012/06/13	Cut-off low	>0.2 km/h	Enhanced
S9	2012/06/13	Cut-off low	>0.2 km/h	Enhanced
S10	2013/08/02	Cut-off low	>0.2 km/h	Enhanced
S11	2013/08/02	Cut-off low	>0.2 km/h	Enhanced

S12	2013/08/03	PV streamer	>0.2 km/h	Enhanced
S13	2013/08/03	PV streamer	>0.2 km/h	Enhanced
S14	2014/01/02	PV streamer	>0.2 km/h	None
S15	2014/01/02	PV streamer	>0.2 km/h	None
S16	2014/01/03	PV streamer	0.1-0.2 km/h	None
S17	2014/01/04	Low/high trough	>0.2 km/h	None
S18	2014/05/02	Low/high trough	0.1-0.2 km/h	Enhanced
S19	2014/05/02	Low/high trough	>0.2 km/h	Enhanced
S20	2015/01/03	PV streamer	>0.2 km/h	None

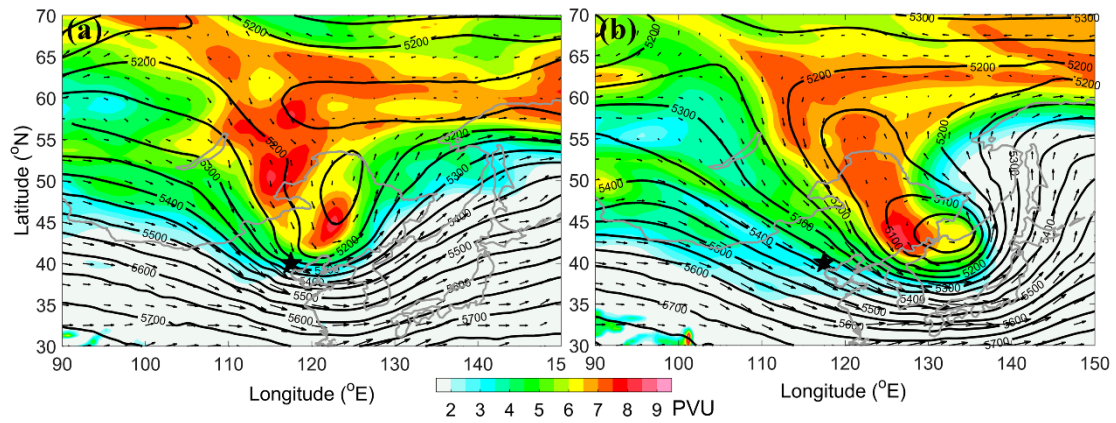
612 **Table 2.** Characteristics of the 20 cases shown in Fig. 11a.

613



615

616 **Figure 1.** Example of the vertical height profiles of (a) the relative radar echo power  
 617 (black line, smoothed by a 3-point running mean) along with its gradient variation  
 618 (orange line), (b) the aspect sensitivity (black line, expressed as the ratio between the  
 619 vertical echo power and oblique echo power) along with its gradient variation (orange  
 620 line), observed on 12 UT 29 November 2014. The vertical profiles of simultaneous  
 621 radiosonde observed temperature and potential temperature gradient are shown in plots  
 622 (c) and (d). The black horizontal line denotes the LRT height derived from the  
 623 radiosonde temperature profile. The orange circle indicates the RT height derived from  
 624 the profile of the radar backscattered echo power.



625

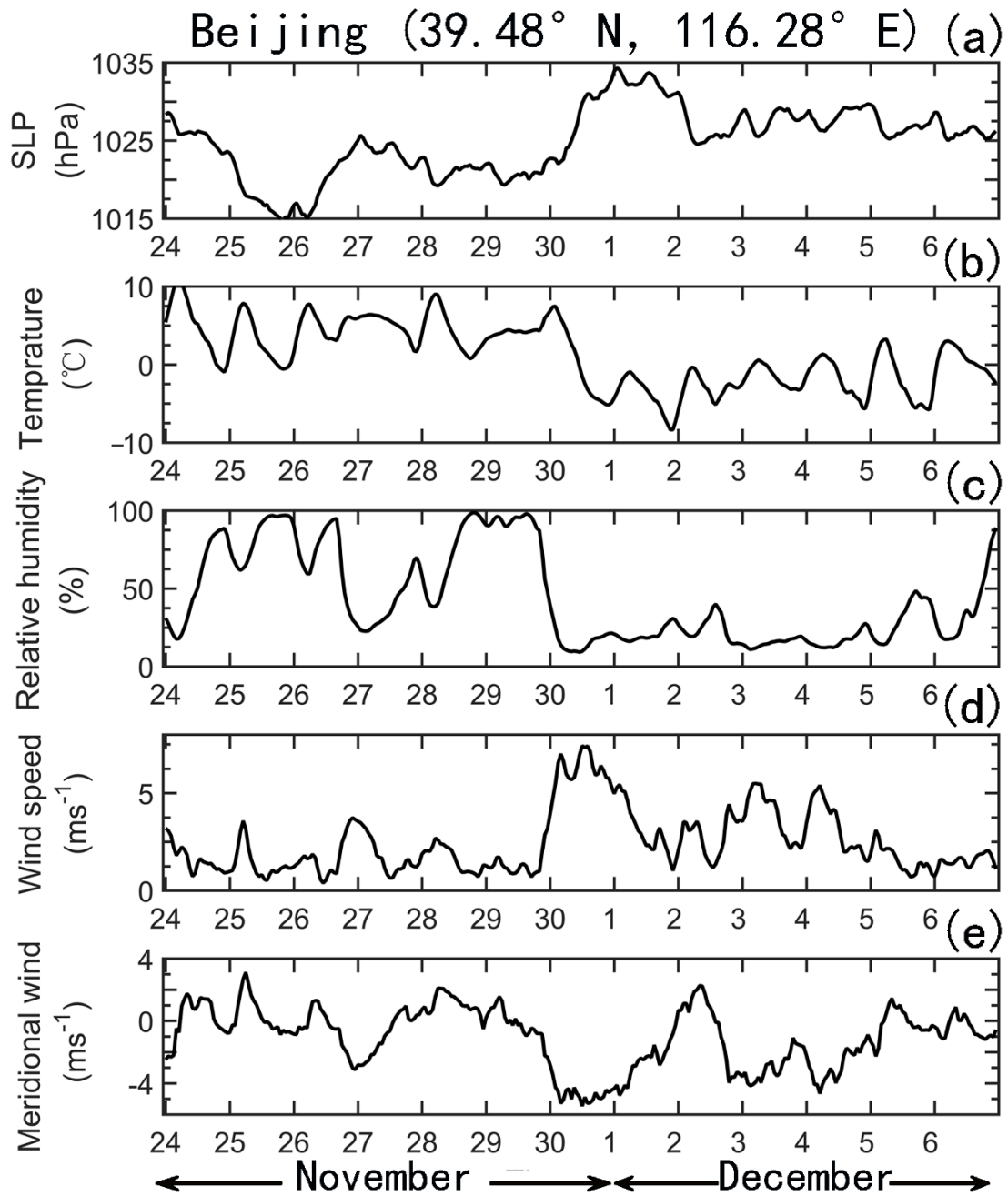
626 **Figure 2.** ECMWF derived isentropic PV map on 315 K surface (shaded above 2 pvu,

627  $1 \text{ PVU} = 10^{-6} \text{ m}^2 \text{ K kg}^{-1} \text{ s}^{-1}$ ) and geopotential height (contoured every 50 m in solid line)

628 along with the wind vector (arrow) at 500 hPa ( $\sim 5.5 \text{ km a.s.l.}$ ) on (a) 18 UTC 30

629 November 2014, (b) 12 UTC 1 December 2014. The black star shows the location of

630 Xianghe.



631

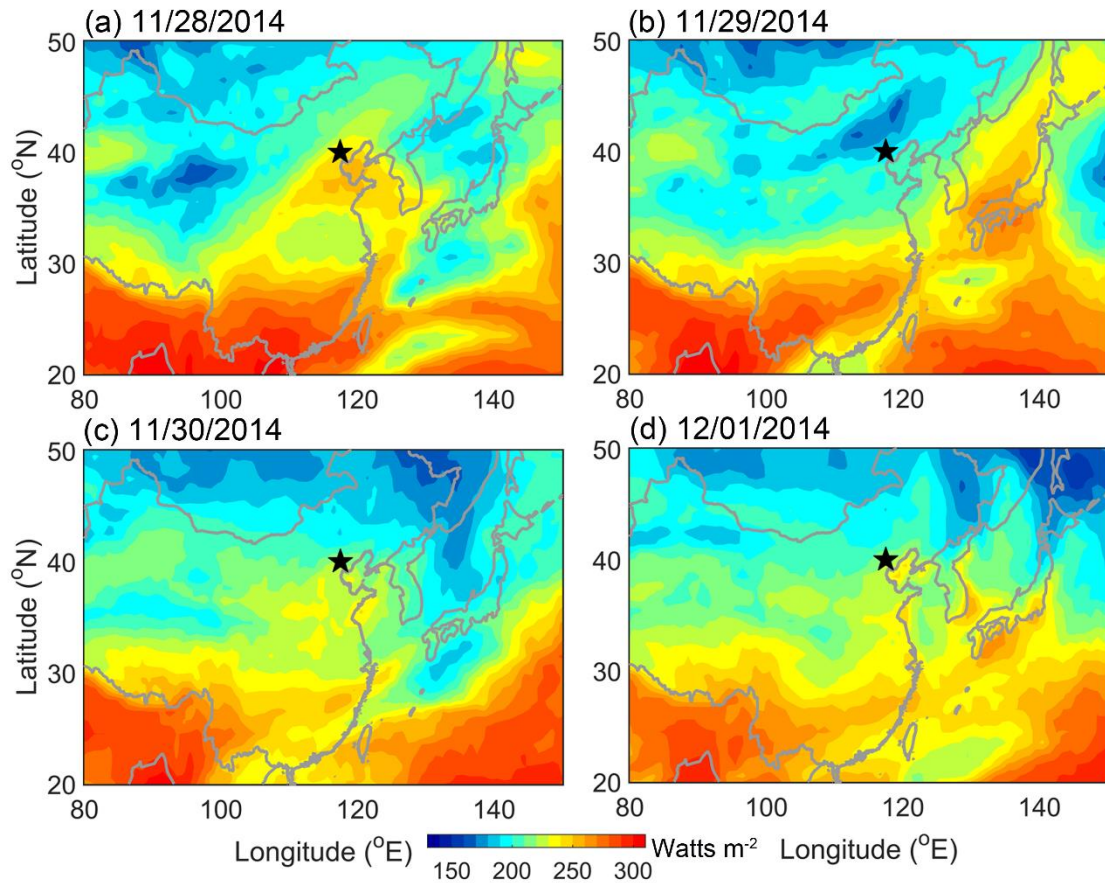
632 **Figure 3.** Time series of surface (~1.2 m above the surface) hourly meteorological

633 measurements of (a) sea level pressure, (b) temperature, (c) relative humidity, (d)

634 horizontal wind, and (e) meridional wind during the period 24 November-6 December

635 2014, observed over the Beijing station (39.4° N, 116.2° E, 31.3 m above sea level).

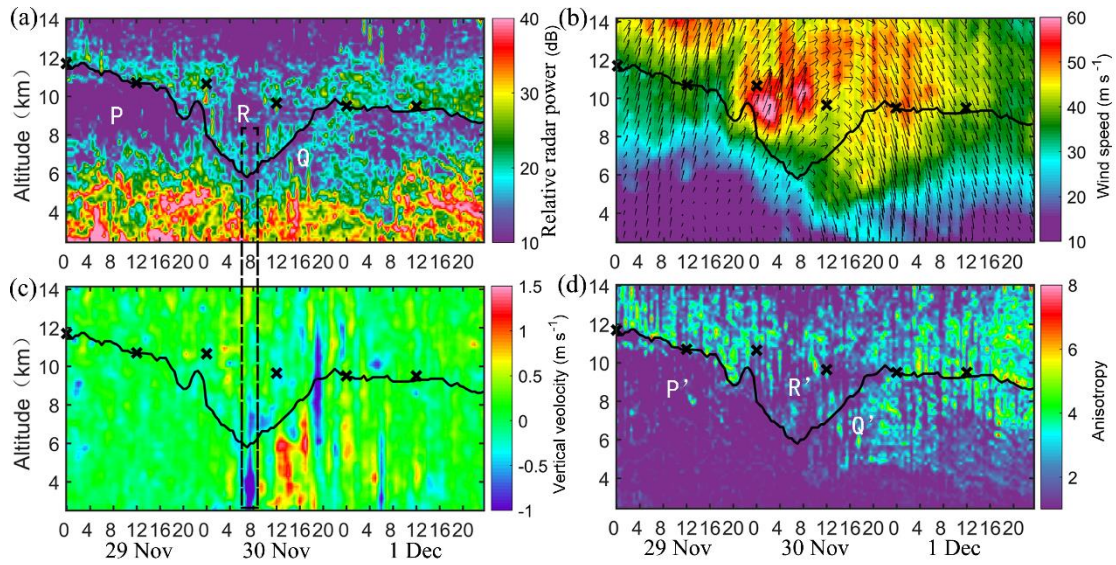
636



637

638 **Figure 4.** Contour maps of the high quality Climate Data Record (CDR) of the daily  
 639 Outgoing Longwave Radiation (OLR), derived from the NOAA high-resolution  
 640 infrared radiation sounder (HIRS) on (a) 28 November, (b) 29 November, (c) 30  
 641 November, and (d) 1 December 2014. The black star shows the location of Xianghe.

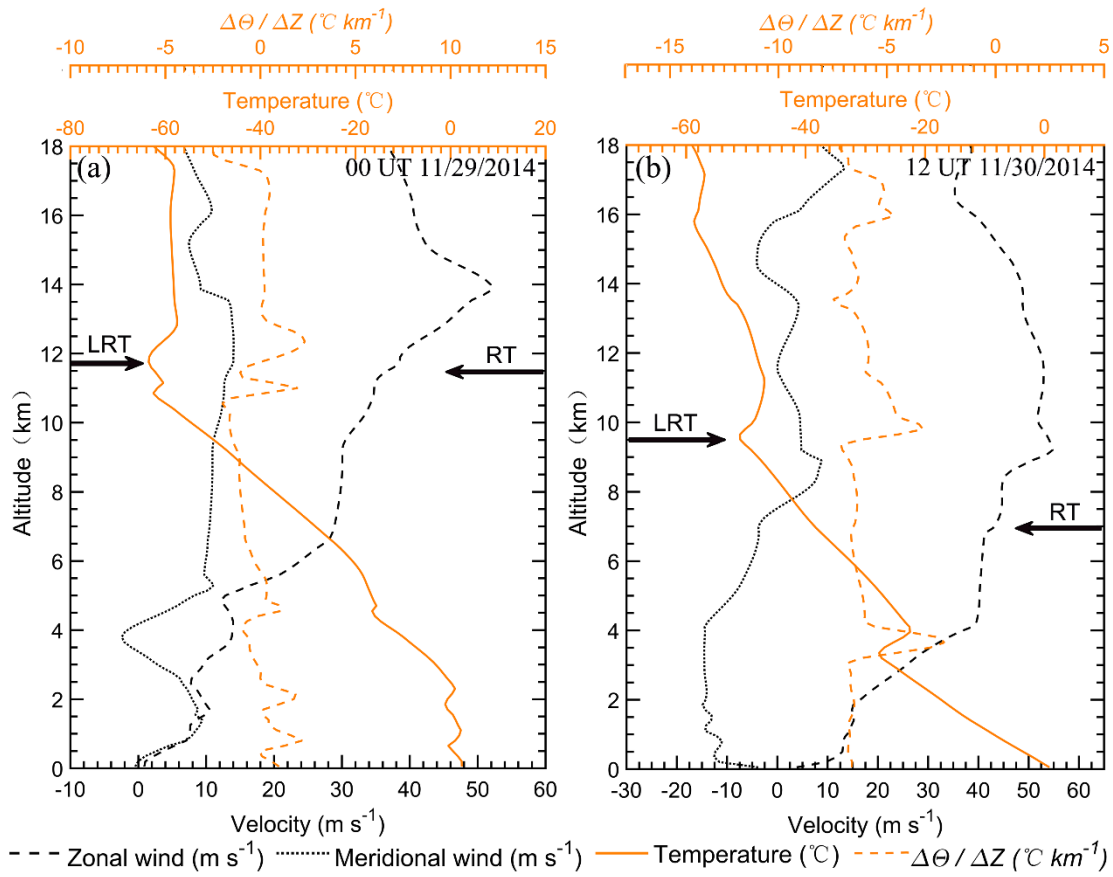
642



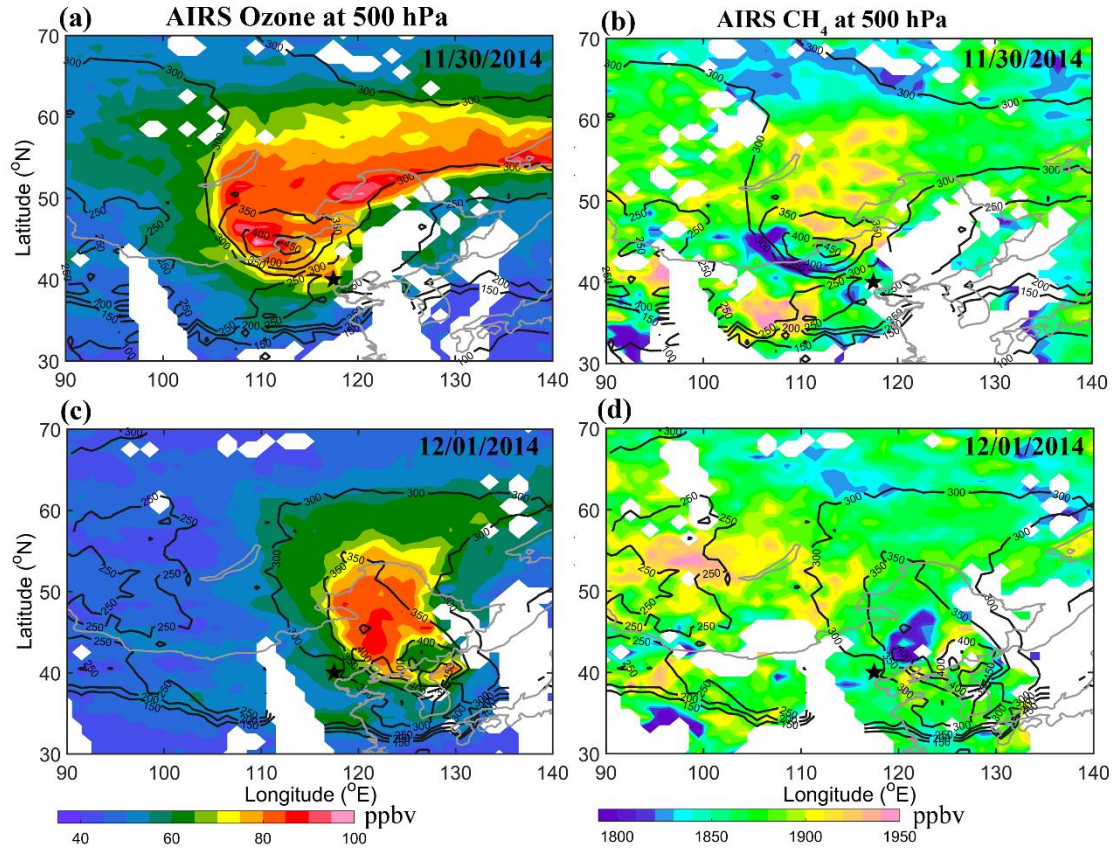
643

644 **Figure 5.** Altitude-time section of (a) the radar backscattered echo power in zenith  
 645 direction, (b) the horizontal wind speed along with wind vector, of which the up and  
 646 down arrows represent north and south respectively, and left-right is west-east, (c) the  
 647 vertical velocity, and (d) the aspect sensitivity, observed by the Beijing MST radar from  
 648 29 November to 1 December 2014. The black curve shows the radar-determined  
 649 tropopause, as defined in section 2.1. The dotted rectangle highlights the strong  
 650 downdrafts immediately preceding the rapid tropopause ascent. The positions of the  
 651 LRT tropopause heights, derived from the nearly simultaneous collocated GPS  
 652 radiosonde temperature profile, are marked by crosses.





653  
 654 **Figure 6.** Vertical profiles of zonal wind, meridional wind, temperature, and potential  
 655 temperature gradient derived from the GPS radiosonde measurements, at (a) 0000 UTC  
 656 29 November 2014 and (b) 1200 UTC 30 November 2014. The bold arrows on the left  
 657 and right side of each panel indicate the radiosonde derived LRT tropopause and radar-  
 658 derived tropopause height, respectively.  
 659



660

661 **Figure 7.** 500 hPa Ozone (left panels) and methane CH<sub>4</sub> (right panels) distribution

662 along with the tropopause height contour, derived from the AIRS satellite observations.

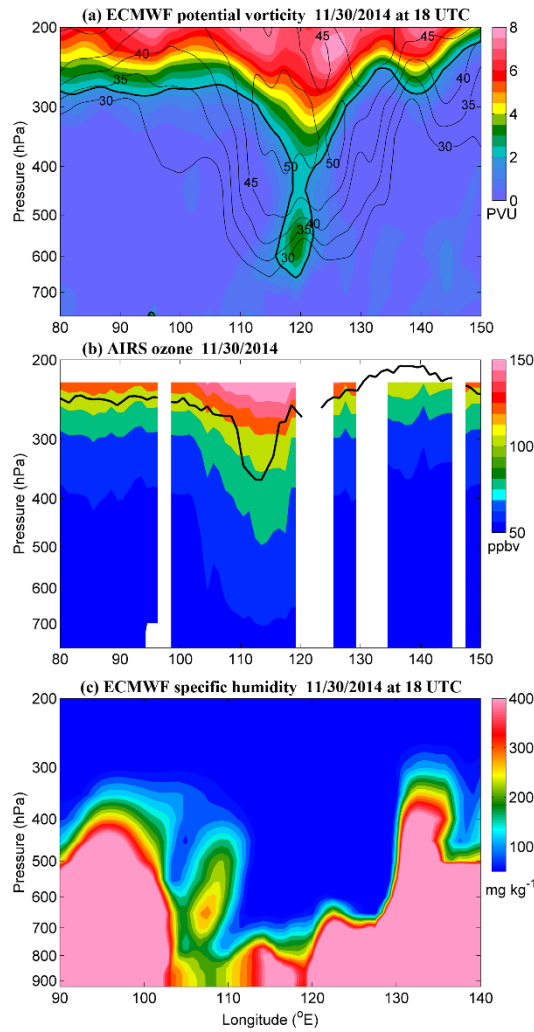
663 The top and bottom plots show the data of 30 November 2014 and 1 December 2014,

664 respectively. According to the Aqua Orbit Tracks (not shown), the time range of the

665 satellite passage is between ~04:00-07:25 on 30 November and between ~03:15-06:35

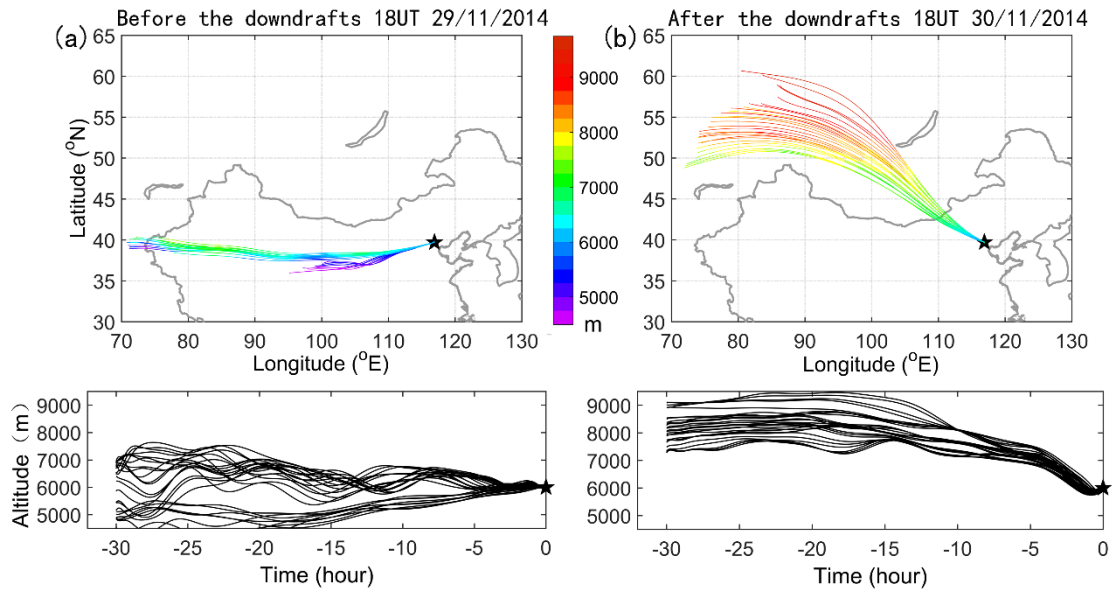
666 on 1 December 2014. The black star indicates the location of Xianghe.

667



668

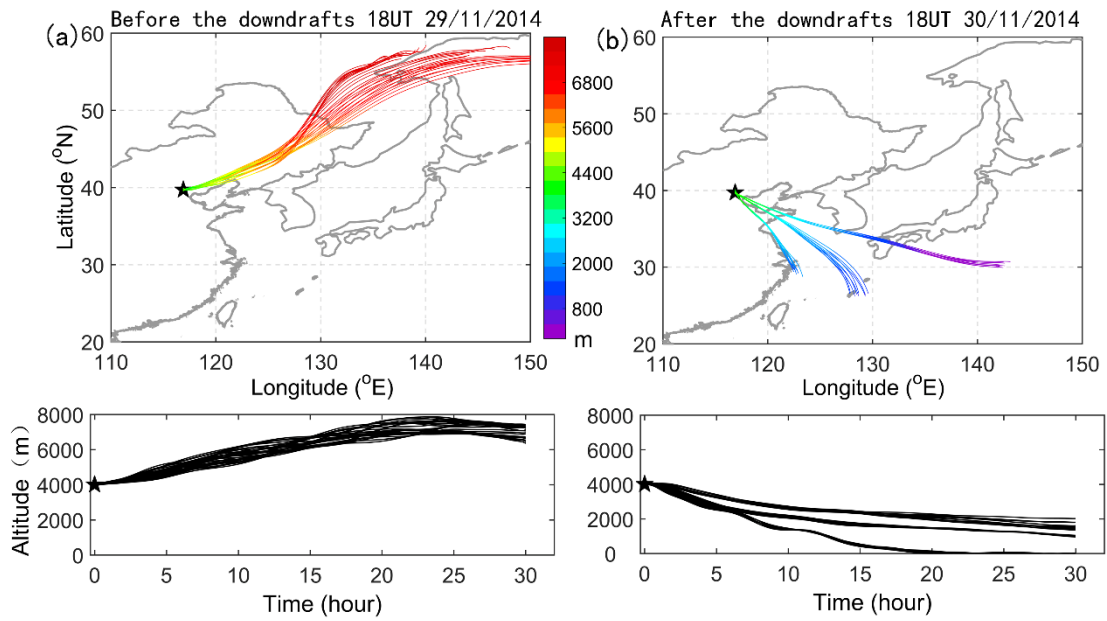
669 **Figure 8.** Longitude-pressure cross section of (a) ECMWF PV (colors, in pvu) along  
 670 with horizontal wind contour (thin black line, m/s) at 18 UTC on 30 November 2014,  
 671 (b) AIRS ozone mixing ratio (colors, in ppbv) along with tropopause height (black line)  
 672 on 30 November 2014, and (c) ECMWF specific humidity (colors, in mg kg<sup>-1</sup>) at 18  
 673 UTC on 30 November 2014, at a constant latitude 40° N (nearest grid point in the  
 674 latitude of Xianghe). The bold line in (a) marks the isotropic line of PV at 2 pvu.



675

676 **Figure 9.** Illustration of 30 h three-dimensional backward trajectories ending at  
 677 Xianghe at 6000 m using National Oceanic Atmospheric Administration (NOAA)  
 678 HYSPLIT model: (a) before the main downdrafts at 18 UTC on 29 November 2014,  
 679 and (b) after the main downdrafts at 18 UTC on 30 November 2014. The HYSPLIT  
 680 ensemble consists of 27 trajectories. Upper plots show the horizontal projection of the  
 681 trajectories, and the lower plots show the corresponding time-height vertical  
 682 displacement of the trajectories.

683

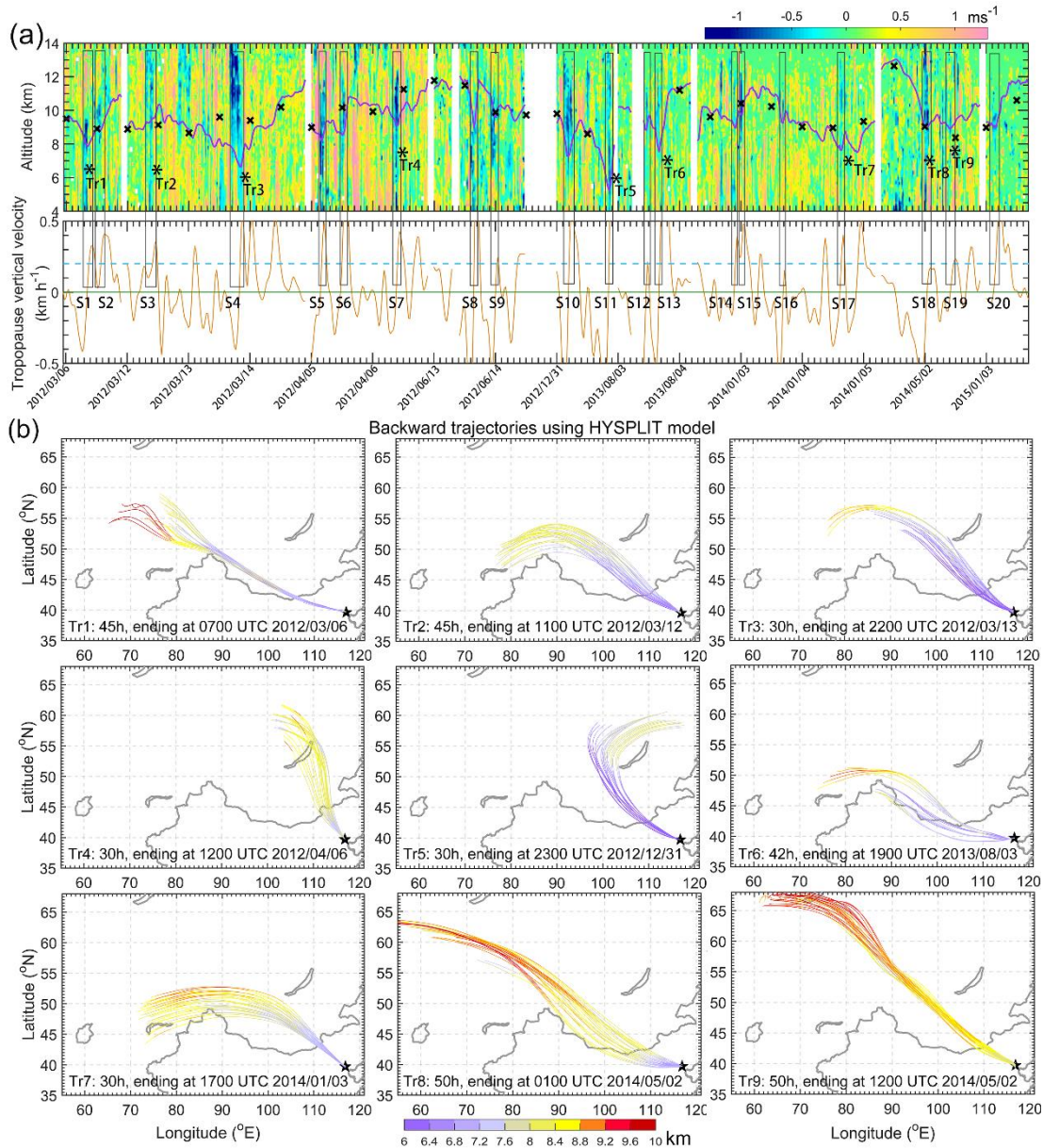


684

685 **Figure 10.** Same as Fig.10 but for three-dimensional forward trajectories starting at

686 Xianghe at 4000 m: (a) before the main downdrafts at 00 UTC on 30 November 2014,

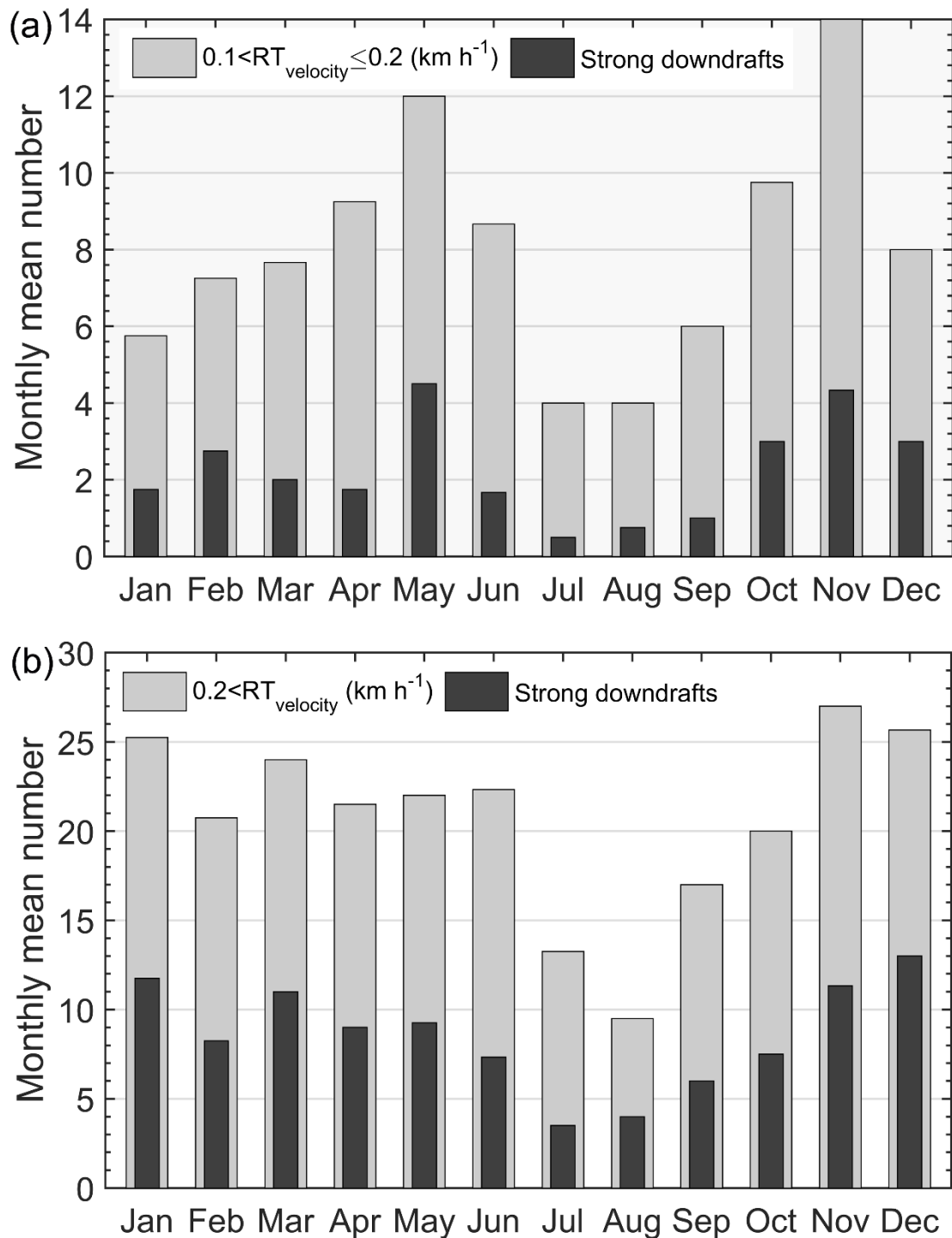
687 and (b) after the main downdrafts at 00 UTC on 1 December 2014.



688

689 **Figure 11.** (a) Height-time section of several episodic observations of the radar-derived  
 690 vertical wind (colors in m/s) along with RT height (purple bold line) and LRT height  
 691 (bold crosses), between March 2012 and Jan. 2015. The corresponding vertical velocity  
 692 of the RT (orange line) is plotted in the lower panel of (a), dotted blue line indicates the  
 693 value of 0.2 km/h. Dates for the observations are displayed as year/month/day. Black  
 694 rectangular boxes represent the cases of strong downdraughts (absolute value  $\geq 0.5$  m/s)  
 695 preceding rapid tropopause ascent ( $>0.1$  km h<sup>-1</sup>) and are labeled as S1, S2, S3..., S20.

696 Symbol ‘\*’ labeled as Tr1-Tr9 indicates the ending point of the corresponding  
697 trajectories in Fig.12b. (b) Results of backward trajectories (colors in km) of the typical  
698 9 selecting cases from Fig.12a, providing the signature and source of possible  
699 stratospheric intrusions.  
700



701

702 **Figure 12.** Four years (2012-2015) of radar-determined monthly mean number of rapid

703 tropopause ascent (gray bands) and the corresponding strong downdrafts just preceding

704 the rapid tropopause ascent (black bands). (a) Gray bands: with the ascent by at least

705 0.6 km and the excursion velocity is between 0.1-0.2 km h<sup>-1</sup>; black bands: except for

706 the criteria of gray bands, strong downdrafts occurred preceding the rapid RT ascent



707 must exceed  $0.5 \text{ m s}^{-1}$  and pass through the RT layer. (b) Same as (a) but for the  
708 occasions when the ascent velocity is larger than  $0.2 \text{ km h}^{-1}$ . According to the study  
709 here, the black bands in the histogram well represent the occurrence of possible  
710 stratospheric intrusions.  
711